International Journal of Thermophysics, Vol. 23, No. 4, July 2002 (© 2002)

Structure and Nonlinear Flow Behavior of Simple and Complex Fluids[1]

S. Hess[2]

The structure of a fluid as described by the pair-correlation function or by the static structure factor is modified by a viscous flow. This modification already exists in the linear flow regime (Newtonian behavior) but it becomes more pronounced at higher shear rates where non-Newtonian effects, such as a dependence of the viscosity on the shear rate and normal stress differences, prevail. Examples are presented for fluids composed of spherical particles, in particular, "simple fluids" and dense colloidal dispersions, and for "complex fluids" composed of nonspherical particles and polymeric chain molecules. Calculations based on kinetic equations for the pair-correlation function or for the orientational distribution function are compared with results obtained by non-equilibrium molecular dynamics (NEMD) computer simulations, as well as with rheological and neutron scattering experiments.

KEY WORDS: colloidal dispersions; nematic liquid crystals; NEMD computer simulations; nonlinear flow behavior; polymer fluids; simple fluids; shear-induced structure; viscosity.

1. INTRODUCTION

The viscosity of "Newtonian fluids" is independent of the shear rate over the experimentally accessible range of shear rates. The shear stress is a linear function of the shear rate. Gases and many liquids, e.g., water, belong to this kind of fluids. A nonlinear flow behavior, also referred to as "non-Newtonian behavior," where the shear stress is a nonlinear function of the shear rate and where consequently the viscosity does depend on the

[1] Invited paper presented at the Fourteenth Symposium on Thermophysical Properties, June 25–30, 2000, Boulder, Colorado, U.S.A.

[2] Institut für Theoretische Physik, Technische Universität Berlin, PN 7-1, Hardenbergstr. 36, D-10623 Berlin, Germany. E-mail: S.Hess@physik.tu-berlin.de

0195-928X/02/0700-0905/0 © 2002 Plenum Publishing Corporation

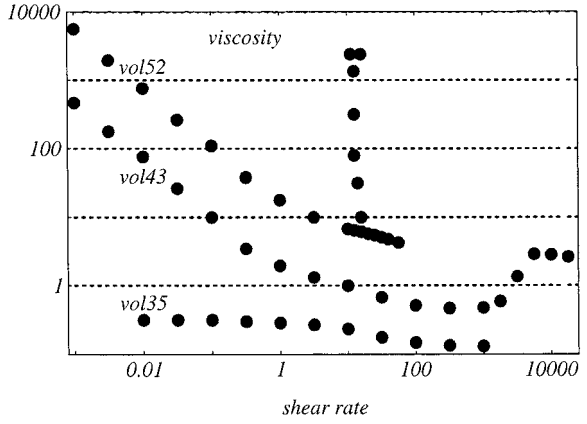

Fig. 1. Viscosity of colloidal dispersions as a function of the shear rate. The labels *vol* 35, *vol* 43, and *vol* 52 refer to solutions where the volume fraction of the spherical colloidal particles is 0.355, 0.434, and 0.523, respectively.

shear rate, is fairly common in complex fluids encountered in the kitchen and in substances of biological and of technical importance, e.g., polymeric liquids, surfactant solutions, colloidal dispersions and liquid crystals. Examples of experimental data obtained for dispersions containing spherical colloidal (latex) particles (diameter 165 nm) with different volume fractions (disolved in glycol) [1] are shown in Fig. 1. Both a decrease (shear thinning) and an increase (shear thickening) of the viscosity can be observed when the shear rates are increased. Also, normal stress differences and volume changes occur in the non-Newtonian flow regime. These are typical nonlinear phenomena.

The nonlinear flow behavior is accompanied by shear-induced structural changes which can be detected by light scattering [2] or by neutron scattering experiments [1, 3]. A complementary method for the study of the dynamical processes involved in the nonlinear flow behavior is provided by "nonequilibrium molecular dynamics" (NEMD) computer simulations. Basic information on this method, some results obtained by it, as well as comparisons with simple model calculations and experiments are presented.

The NEMD computer simulations devoted to the study of transport and relaxation processes in fluids have been developed over twenty-five years ago [4]. By now the method is well established [5–10]. During the last decade the emphasis was, on the one hand, on the investigation of physical phenomena in simple fluids far away from equilibrium, i.e., typical nonlinear phenomena, and, on the other hand, on the study of the material properties of complex fluids.

A plane Couette flow, also referred to as "simple shear flow," is considered as an example of a stationary transport process. The method of NEMD simulations is firstly discussed for fluids composed of spherical particles. It turns out that the flow behavior of the so-called simple fluids and the shear-induced structural changes are not simple. A comparison with experimental results of (dense) colloidal dispersions of spherical particles is made. The complex fluids to be discussed here are nematic liquid crystals and polymeric fluids.

2. FLUIDS OF SPHERICAL PARTICLES

2.1. Molecular Dynamics

In a molecular dynamics computer simulation *Newton's equations of motion* $m\frac{d^2}{dt^2}\mathbf{r}^i = \mathbf{F}^i = \sum_j \mathbf{F}^{ij}$ are integrated numerically for N particles with mass m, located at positions $\mathbf{r}^i$ in a volume V. The particle density is $n = N/V$. The particle i, $(i = 1, 2, ..., N)$, feels the force $\mathbf{F}^i = \sum_j \mathbf{F}^{ij}$ which is the sum of the forces $\mathbf{F}^{ij}$ exerted by all other particles $j \neq i$ on particle i.

Surface effects are avoided when one uses periodic boundary conditions and the nearest image convention. This means, particle i either feels the force caused by particle j or by one of its images depending on which one is closest to it. The range of the force has to be shorter than half of the length of the basic (central) periodicity box. The temperature T is linked with the kinetic energy: $\frac{3}{2}k_B T = N^{-1}\frac{1}{2}\sum_i m(\mathbf{c}^i)^2$, where k_B is the Boltzmann constant and $\mathbf{c}^i$ is the "peculiar velocity," i.e., the velocity of a particle relative to the flow velocity. To simulate an isothermal system, the temperature has to be kept constant. The simplest version of a "thermostat" consists in rescaling the peculiar velocity after each time step by the factor $(T_{\text{wanted}}/T_{\text{measured}})^{1/2}$. This is equivalent to using the "Gaussian" thermostat. Other thermostats, e.g., that one associated with the names Nosé and Hoover are discussed in Refs. 5–10, see also the studies of Evans and Morriss on thermostatting [11].

A typical binary interaction potential Φ depending on the distance r is the *Lennard–Jones* (LJ) potential $\Phi = \Phi^{LJ} := 4\Phi_0((\frac{r_0}{r})^{12} - (\frac{r_0}{r})^6)$. In the simulations dimensionsless or "scaled" variables are used which are denoted by the same symbols as the physical variables when no danger of confusion exists. For a system of LJ-particles, lengths and energies are presented in units of the diameter r_0 and of the potential depth Φ_0. The units used for the particle density and for the temperature are r_0^{-3} and $k_B^{-1}\Phi_0$. The time is scaled with the reference time $t_0 = r_0 m^{1/2}\Phi_0^{-1/2}$, m is the mass of a particle. The pressure, the shear rate and the viscosity of the

LJ-fluid are expressed in units of $r_0^{-3}\Phi_0$, t_0^{-1} and $r_0^{-3}\Phi_0 t_0 = r_0^{-2}m^{1/2}\Phi_0^{1/2}$. When only the repulsive r^{12}-part of the LJ interaction potential is taken into account one speaks of a "soft spheres" (SS) potential. The LJ-potential cut off at its minimum $rr_0^{-1} = 2^{1/6} \approx 1.1225$ which is also purely repulsive, is referred to as the WCA-potential. A variety of other potentials have been used but the LJ-potential sets a standard for short range potentials.

The observables of interest, such as the internal energy, the components of the pressure or the stress tensor, as well as the velocity distribution function, the pair correlation function or the static structure factor can be calculated from the known positions and velocities of the particles as time averages according to the rules of statistical physics. In nonequilibrium molecular dynamics (NEMD) simulations transport and relaxation phenomena are investigated in close analogy to real experiments. States far away from equilibrium are also studied.

2.2. Plane Couette Flow

For a simple shear flow in the x-direction with the gradient in the y-direction, the shear rate γ is given by $\gamma = \frac{\partial v_x}{\partial y}$. Such a flow can be either generated by moving boundaries or by forces [4, 7], or as used here, by moving image particles undergoing an ideal Couette flow with the prescribed shear rate (homogeneous shear). The periodic boundary conditions for the particles leaving and entering the basic box have to be modified (Lees–Edwards boundary conditions [5]). For a system in a fluid state in equilibrium and for shear rates not too large, a linear velocity profile typical for a plane Couette flow is set up in the basic box (from which the data are extracted). At high shear rates where also plug-like flow occurs it is essential to use a velocity "profile unbiased thermostat" (PUT, [5, 12]). A shear flow can also be generated by modifying the equations of motion (SLLOD [5]).

2.3. Viscosity and other Rheological Properties

Rheological properties such as the (non-Newtonian) viscosity and the normal pressure differences are obtained from the cartesian components of the stress tensor $\sigma_{\mu\nu} = -p_{\mu\nu}$ or of the pressure tensor $p_{\mu\nu}$ which is the sum of "kinetic" and "potential" contributions: $p_{\mu\nu} = p_{\mu\nu}^{\text{kin}} + p_{\mu\nu}^{\text{pot}}$, where $Vp_{\mu\nu}^{\text{kin}} = \sum_i m_i c_\mu^i c_\nu^i$, $Vp_{\mu\nu}^{\text{pot}} = \frac{1}{2}\sum_{ij} r_\mu^{ij} F_\nu^{ij}$. Here $\mathbf{c}^i$ is the peculiar velocity of particle i, i.e., its velocity relative to the flow velocity $\mathbf{v}(\mathbf{r}^i)$, $\mathbf{r}^{ij} = \mathbf{r}^i - \mathbf{r}^j$ is the relative position vector of particles i, j and $\mathbf{F}^{ij}$ is the force acting between them. The Greek subscripts μ, ν which assume the values 1, 2, 3 stand for cartesian components associated with the x, y, z-directions. In the

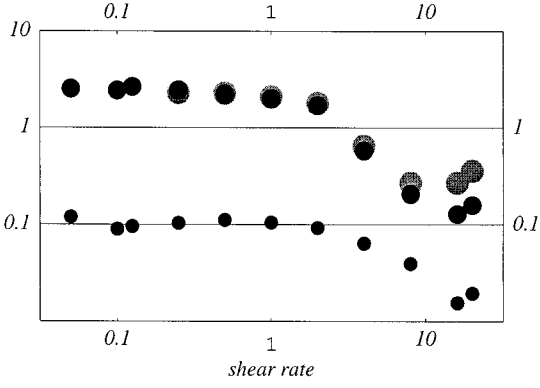

Fig. 2. The kinetic (small points) and potential (large black points) contributions to the viscosity $\eta = -p_{yx}/\gamma$, as well as the total viscosity inferred from the entropy production (large gray points), for a LJ-fluid as functions of the shear rate γ.

simulations, the expression for the pressure tensor given is averaged over many (10^3 to 10^6) time steps.

For the present flow geometry, the (non-Newtonian) viscosity η is obtained by dividing the $yx(21)$-component of the stress or pressure tensor by the shear rate γ, viz.: $\eta = \sigma_{yx}/\gamma = -p_{yx}/\gamma$. The kinetic and potential contributions to the pressure tensor and to the viscosity can be computed seperately from the simulation. Only the sum can be measured in a real experiment. The kinetic contribution to the viscosity is the dominating one in dilute gases [6]. In dense fluids (liquids) the potential contribution is the more important one, cf. Fig. 2. The data shown stem from simulations with $N = 512$ particles [8], the interaction has been cut off at $r = r_c = 2.5r_0$. The density $n = 0.84r_0^{-3}$ corresponds to the triple point density, the temperature $T = \Phi_0/k_B$ is somewhat higher than the tripel point temperature. Normal stress or pressure differences, e.g., $\sigma_{xx} - \sigma_{yy} = p_{yy} - p_{xx}$ can be computed analagously. In Fig. 2 the total vicosity is also shown as it follows from the entropy production which is proportional to $\eta\gamma^2$ and is determined by the heat removed from the system by the thermostat.

2.4. Structural Changes in the Various Flow Regimes

2.4.1. Qualitative Discussion

The shear rate dependence of the viscosity as displayed in the "flow curve" Fig. 2 shows four regimes: (I) The *Newtonian flow* regime where the shear viscosity η is independent of the shear rate γ and where normal

pressure differences practically vanish. In the present case the Newtonian regime corresponds to $\gamma < 0.1$ (in LJ units). (II) A *weak shear thinning* for $0.2 < \gamma < 2$. (III) A *strong shear thinning* for $2 < \gamma < 20$. (IV) Indications for a *shear thickening* for $\gamma > 20$.

These qualitative differences of the flow behavior are linked with different flow induced structural changes in the fluid. In regimes (I) and (II) these can be noticed in the pair correlation function $g(\mathbf{r})$ or equivalently, in its spatial Fourier transform, the static structure factor $S(\mathbf{k})$ which determines the scattering intensity. Both quantities become anisotropic in the presence of a viscous flow. The structure factor shows distorted Debye–Scherrer rings. In regime (III) a long range partial positional ordering takes place which is apparent in real space and it is evident in snapshots [17, 18]. Of course, the long range ordering is also seen in $g(\mathbf{r})$ and it leads to Bragg-like peaks in $S(\mathbf{k})$, cf., Refs. 1, 12, and 13.

Above, the various flow regimes have been distinguished by the shear rate expressed in LJ-units. The physically relevant variable, however, is the product $\gamma\tau$ of the shear rate and the Maxwell relaxation time τ which, in turn, is given by the small shear rate limit of the ratio η/G, i.e., of the viscosity and the (high frequency) shear modulus G. The latter quantity, which can also be extracted from the simulation, is approximately 25 for the present system and the relaxation time is $\tau \approx 0.1$ in LJ units. Thus non-Newtonian flow phenomena can be observed for $\gamma > 0.1\tau^{-1}$. In simple fluids like liquid argon this corresponds to a shear rate which is several orders of magnitude larger than $10^6\,\mathrm{s}^{-1}$ which can reasonably be reached in laboratory experiments. The situation is different in (dense) colloidal dispersions of spherical particles. There, considerably longer relaxation times occur and non-Newtonian effects can be noticed and are of importance for many applications.

The potential part of the pressure tensor is also determined by an integral over the pair correlation function g:

$$p_{\mu\nu}^{\mathrm{pot}} = \tfrac{1}{2} n^2 \int r_\mu F_\nu \, g(\mathbf{r}) \, d^3r. \tag{1}$$

Here $\mathbf{F}$ is the force acting between two particles. Equation (1) is the basis for the strong dependence of the viscous properties on the structure of a fluid.

2.4.2. *Generalized Stokes–Maxwell Model*

The structural changes in the flow regimes I and II can be treated by starting from a Kirkwood–Smoluchowski type of kinetic equation [14–16] for the pair correlation function $g = g(\mathbf{r})$:

$$\partial g/\partial t + \gamma r_y \, \partial g/\partial r_x + \mathscr{D}(g) = 0. \tag{2}$$

Here, $\mathbf{r}$ is the relative position vector between an arbitrary reference particle and any other particle in the fluid. The "damping" term $\mathscr{D}(g)$ ensures that g approches the equilibrium pair correlation function g_{eq} which is also referred to as the radial distribution function. With the relaxation time approximation $\mathscr{D}(g) = \tau^{-1}(g - g_{\text{eq}})$, where τ is the Maxwell relaxation time, and for a stationary situation, the kinetic equation is equivalent to $g = g_{\text{eq}} - \gamma\tau r_y \, \partial g / \partial r_x$. Iteration of this equation leads to a power series in $\gamma\tau$, the first few terms are

$$g = g_{\text{eq}} - \gamma\tau r_x r_y r^{-1} g'_{\text{eq}} + (\gamma\tau)^2 (r_y^2 r^{-1} g'_{\text{eq}} + r_x^2 r_y^2 r^{-1} (r^{-1} g'_{\text{eq}})') - \cdots + \cdots. \quad (3)$$

Here, the prime denotes differentiation with respect to $r = |\mathbf{r}|$. Notice that g_{eq} depends on r but not on the angles specifying the direction of the vector $\mathbf{r}$. The power series expansion, Eq. (3), is referred to as the generalized Stokes–Maxwell model [15].

According to the linear Stokes–Maxwell relation, the difference between the pair correlation functions g_{45} and g_{135} along the lines in the x–y plane which enclose the angles of 45 and 135° with the x-axis, i.e., the function $g_+ = g_{45} - g_{135}$, is given by $-\gamma\tau r g'_{\text{eq}}$. In Fig. 3, this relation is tested for a Lennard-Jones liquid at the same temperature and density as used for the data presented in Fig. 2. The shear rate $\gamma = 0.125$ is in the linear flow regime. The relaxation time τ has been set equal to 0.14. The large gray dots mark the values of g_+ as directly extracted from the simulation, the

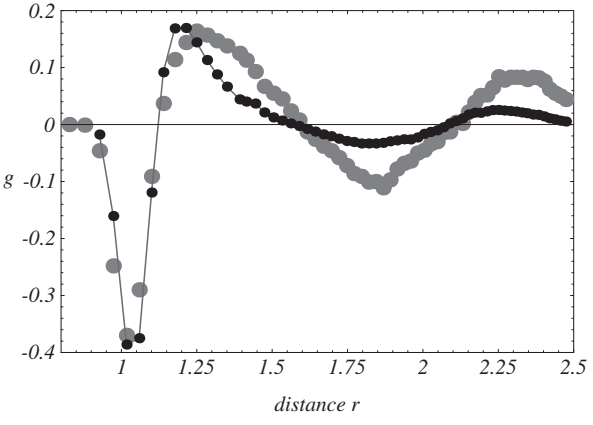

Fig. 3. Test of the Stokes–Maxwell relation for a Lennard–Jones liquid in the linear flow regime. Data directly obtained in the NEMD simulation (large gray dots) are compared with those computed via the Stokes–Maxwell relation (small black dots connected by lines). The density, temperature, and shear rate are $n = 0.84$, $T = 1.0$, and $\gamma = 0.125$ (in LJ units), the relaxation time $\tau = 0.14$ was used.

small black dots connected by lines are the same quantity computed via the Stokes–Maxwell relation. Though the agreement is far from perfect, the essential features are described rather well.

The stationary solution of Eq. (2) can be written in closed form as $g = \int_0^\infty e^{-\alpha} g_{\mathrm{eq}}\,(r_x - \alpha\,\gamma\tau\,r_y, r_y, r_z)\,d\alpha$. For the static structure factor $S = S(\mathbf{k})$ which is essentially the Fourier transform of $g-1$, a power series expansion similar to Eq. (3) is obtained where, however, the components k_y and k_x of the scattering wave vector $\mathbf{k}$ play the role of r_x and r_y. The solution in closed form is

$$S = \int_0^\infty e^{-\alpha} S_{\mathrm{eq}}(k_x, k_y + \alpha\gamma\tau k_x, k_z)\,d\alpha. \tag{4}$$

To demonstrate the basic features of the influence of the shear flow on the structure as described by Eq. (4) the simple model expression $1 - 0.96\exp(-k^2/10) + S_{\max}(k^2\exp(1-k^2))^4$, with $S_{\max} = 2.6$, is used as an approximation for S_{eq} in the vicinity of its first maximum occurring at $k = 1$. The contour graphs in Fig. 4 show $S(\mathbf{k})$ in the k_x–k_y plane in equilibrium (left) and for a plane Couette flow with $\gamma\tau = 0.1$ (right). This shear rate is in the linear or Newtonian flow regime. Under shear, the Debye–Scherrer ring is elliptically distorted and its long axis encloses the angle $-45°$ (or 135°) with the flow direction. In Fig. 5, $S(\mathbf{k})$ is displayed in the k_x–k_y plane (left) and k_x–k_z plane (right) for $\gamma\tau = 0.5$. The shear rate is in the weak shear thinning regime. Nonlinear effects are the modulation of the intensity around the Debye–Scherrer rings and the rotation of the long axis of the ellipse in the k_x–k_y plane from the diagonal towards the y-axis.

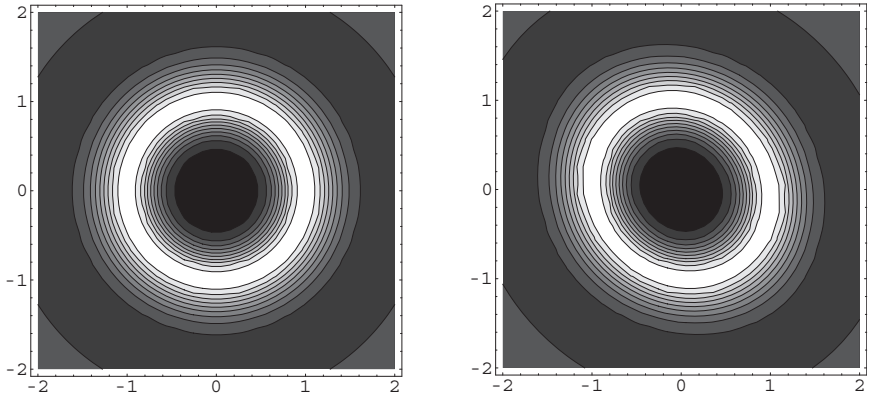

Fig. 4. Static structure factor $S(\mathbf{k})$ in the k_x–k_y plane, in equilibrium (left) and under shear with $\gamma\tau = 0.1$ (right), corresponding to the linear or Newtonian flow regime. Bright (dark) regions indicate high (low) intensities. The flow velocity is in the horizontal (x) direction.

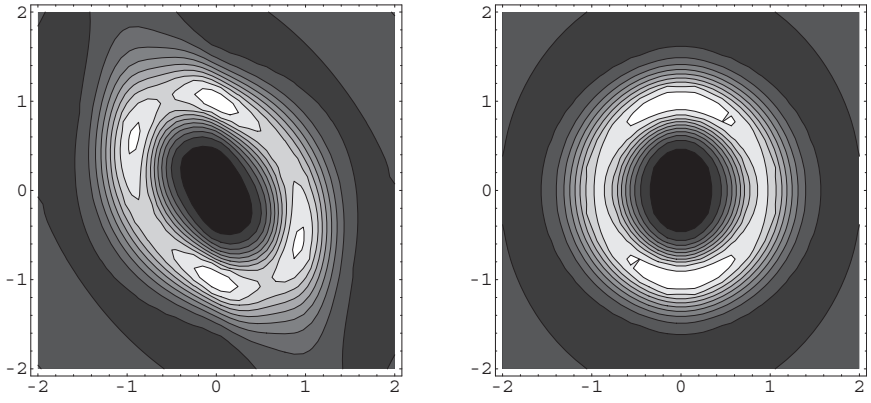

Fig. 5. Static structure factor $S(\mathbf{k})$ in the k_x–k_y plane (left) and in the k_x–k_z plane (right) for $\gamma\tau = 0.5$, corresponding to the nonlinear, weak shear thinning flow regime. The flow velocity is in the horizontal (x) direction.

2.4.3. Long-Range Partial Positional Ordering

A long-range partial positional ordering, in particular the formation of layers and strings of particles, has been found in the simulations [17, 18] for shear rates where a strong shear thinning occurs. Although actual snap shots of the positions of the particles depend on the details of the simulation and are affected by the boundary conditions [12], the phenomenon as such seems to be generic.

Dense colloidal dispersions of spherical particles exhibit flow curves, cf. Fig. 1, which are qualitatively similar to those presented above. In the extreme shear thinning regime III where partial positional order is observed in the NEMD simulations, the static structure factor as measured in small angle neutron scattering (SANS) experiments agrees very well with that computed from NEMD [1].

In Fig. 6 the static structure factor in the plane normal to the direction of the velocity gradient is shown for the SANS experiment (left) and the NEMD simulation [12] for a soft-sphere fluid (right). In the latter case, the form factor of the spherical particles with the known radius (0.55 in reduced units) has been taken into account. The dispersion corresponds to the substance labelled by *vol* 43 in Fig. 1, it was subjected to a Couette flow with a shear rate of 1 s^{-1}.

In addition to the forces acting between the colloidal particles, the friction and the (Brownian) fluctuating forces caused by the background fluid have to be taken into account in colloidal dispersions. For a comparison of viscous properties computed by NEMD simulations with those obtained by "Brownian dynamics" see Ref. 10.

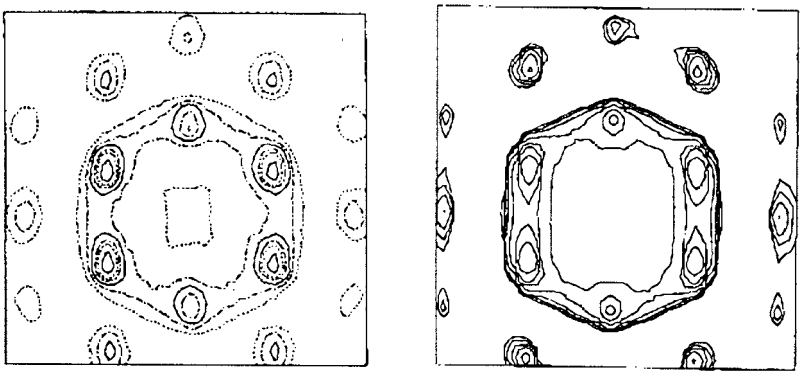

Fig. 6. Static structure factor in the plane normal to the direction of the velocity gradient for the SANS experiment (left) and the NEMD simulation (right).

The generalized Stokes–Maxwell model dicussed above does not apply to the flow regimes III and IV. Though a better understanding of the dynamic processes in these regimes is needed, the transition from the weak to the strong shear thinning can be inferred from a stability analysis within a generalized hydrodynamic theory [12].

MOLECULAR FLUIDS

3.1. General Remarks

A shear flow affects the orientation of molecules. This holds true for all molecular fluids and fluids composed of nonspherical particles. The flow birefringence, looked for and discovered by Maxwell [19], provides evidence for the shear-induced alignment of (optically) anisotropic particles. The effect is particularly strong in liquid crystalline phases. The competition between the flow and the orientation caused by applied electric or magnetic fields leads to dramatic changes of the viscosity. Non-Newtonian effects are strong in polymeric fluids where chain molecules are not only oriented but also deformed by a flow. The rheological behavior of polymeric melts and for configurational changes in melts and in dilute polymer solutions are discussed.

3.2. Nematic Liquid Crystals

3.2.1. Director and Order Parameter of Nematics

Liquid crystals are substances composed of nonspherical particles. The nematic phase is distinguished from the isotropic phase by the existence of

a nonvanishing second rank alignment tensor [20]. In equilibrium and outside the core of defects, the alignment tensor of (ordinary) nematic liquid crystals is uniaxial. Then it is charcterized by a unit vector parallel to its symmetry axis, the "director" **n**, and by its magnitude, the Maier–Saupe order parameter S. This quantity is the average of the second Legendre polynomial depending on the angle between the axis **u** of a molecule and the average preferential direction **n**: $S = \langle P_2(\mathbf{u}\cdot\mathbf{n})\rangle$. The bracket $\langle\ldots\rangle$ indicates an average to be evaluated with an orientational distribution function. The directions **n** and $-\mathbf{n}$ are physically equivalent. In the isotropic phase in equilibrium and in the absence of orienting external fields, one has $S = 0$. In the nematic phase, one has $S \approx 0.4$, close to the isotropic–nematic transition temperature. At lower temeratures, S increases to approximately 0.7 to 0.8, before a transition to a smectic or a solid phase takes place. Perfect orientation corresponds to $S = 1$. Except for temperatures very close to the isotropic–nematic phase transition, the order parameter S is not affected by a flow. The director **n**, however, strongly "feels" torques caused by the velocity gradient. This situation, uniaxial alignment with constant order parameter, but variable director, is described by the Ericksen–Leslie theory [20, 21].

3.2.2. External Orienting Field

An external magnetic field **B**, with $B = |\mathbf{B}|$ exerts the torque (density) $\mu_0^{-1}\chi_a \mathbf{n}\times\mathbf{B}\,\mathbf{n}\cdot\mathbf{B}$ on the nematic liquid crystal. Here $\chi_a = \chi_\parallel - \chi_\perp$ is the difference between the magnetic susceptibilty for the field parallel and perpendicular, to the director **n**. The torque caused by the shear rate γ is characterized by the Leslie viscosity coefficients γ_1 and γ_2. For a stationary Couette flow with a field applied in the y-direction, the torque balance yields $\gamma(\gamma_1 + \gamma_2 \cos 2\varphi) = \mu_0^{-1}\chi_a B^2 \sin 2\varphi$. The director lies in the xy-plane and encloses the angle φ with the flow direction. With

$$\tilde{B}^2 = \mu_0^{-1}\chi_a B^2/(\gamma_1\,\gamma), \tag{5}$$

the solution of this equation is

$$\cos 2\varphi := c_w = c_0(1-\tilde{B}^2\sqrt{1-c_0^2+c_0^2\tilde{B}^4})/(1+c_0^2\tilde{B}^4),\quad c_0 = -\gamma_1/\gamma_2. \tag{6}$$

This relation is equivalent to $\tilde{B}^2 = (1-c_w/c_0)/\sqrt{1-c_w^2}$. Notice that $c_w = 0$, corresponding to the director oriented parallel to the bisector between the x and y axes, implies $\tilde{B} = 1$. The effective viscosity

$$\eta_{2,\,\mathrm{eff}}(\tilde{B}) = \tfrac{1}{2}(\eta_1+\eta_2) + \tfrac{1}{2}(\eta_1-\eta_2)\,c_w + \tfrac{1}{4}\eta_{12}\,(1-c_w^2) \tag{7}$$

depends on the strength of the applied field via $c_w = \cos 2\varphi$. Here η_1 and η_2 are the Miesowicz viscosity coefficients for the director oriented parallel to the directions of the velocity ($\varphi = 0$) and of its gradient ($\varphi = \pi/2$), repectively. The viscosity for the case where **n** is parallel to the bisector between the x- and y-axes ($\varphi = \pi/4$) is denoted by η_4. The Helfrich viscosity η_{12} is given by $\eta_{12} = 4\eta_4 - 2(\eta_1 + \eta_2)$. In typical nematics, η_2 is larger than η_1 by a factor of 5 to 10, η_{12} can have either sign. The Leslie coefficient $\gamma_2 = \eta_1 - \eta_2$ is negative for ordinary nematics. For $B = 0$, the free flow viscosity η_{free} is found from Eq. (7). Usually, the (free) flow alignment angle is small, then η_{free} is not much larger than η_1. The Miesowicz viscosity η_2 is reached for $\tilde{B}^2 \gg 1$, i.e., for $\mu_0^{-1}\chi_a B^2 \gg \gamma_1\, \gamma$, where $c_w \to -1$. Here $\chi_a > 0$ is assumed. A fit of the effective viscosity for intermediate values of the applied field can be used to determine the three viscosity coefficients η_1, η_2, and η_{12}, as well as γ_1 from a single flow geometry.

3.2.3. The Gay–Berne Potential

A model of liquid crystals, which captures many features of the mesogenic behavior, is the Gay–Berne potential [22, 23]. It is a Lennard–Jones type potential where the shape of the particles and the energy depth are anisotropic.

Extensive studies of the equilibrium properties of the Gay–Berne fluid have been performed for different values of the potential parameters, densities and temperatures, e.g., see Refs. 23 and 24. Computation of the viscous properties, however, has been made for just a few selected values of the model parameter and state points, using NEMD methods [25, 26] and the integrals over time correlation functions from MD simulations [27].

NEMD simulations both for a perfectly oriented Gay–Berne fluid [28] and for the case where an external field affects the orientation of the directorhave been performed. As in many studies, particles had an axis ratio 3 and a well-depth ratio for side-side and end-end configurations of 5. The interaction potential was cut off at the distance $r = 4.5r_0$. In previous studies [29], the main motivation was to analyze the pre-smectic increase of the viscosity in the nematic phase as revealed by comparing results for various densities and temperatures. Here results are presented for the field dependence at a state point where these pre-smectic effects are not relevant. To be more specific, the density and temperature are 0.32 and 0.95, respectively, in reduced units. The temperature was kept constant by thermostatting the translational degrees of freedom.

3.2.4. Simulation Results and Fit Curves

In Fig. 7 simulation data and a fit curve for the cosine of twice the flow alignment angle $\cos 2\phi$ are shown as a function of the orienting field B

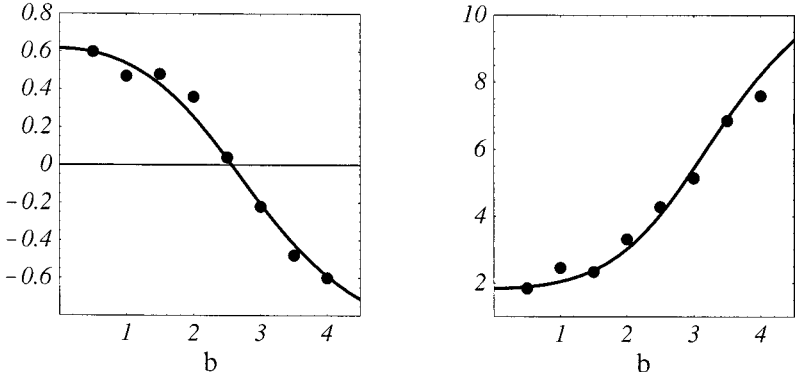

Fig. 7. Cosine of twice the flow alignment angle (left) and the effective viscosity (right) as functions of the reduced field strength b (L. Bennett).

for the shear rate $\gamma = 0.05$. In the plot the variable $b = \tilde{B}(\gamma_1)^{1/2}$ is used which is the magnitude of the field in units of $(\gamma\mu_0/\chi_a)^{1/2}$. The angle ϕ varies from about 25° with no field applied to around 60° at the highest field strength. The values 6.6 ± 0.3 and -10.7 ± 0.6 for the viscosity coefficients γ_1 and γ_2, respectively, are obtained by fitting the data according to Eq. (6). The fit of the effective viscosity yields $\eta_1 = 1.3 \pm 1.0$, $\eta_2 = 12.0 \pm 1.6$ and $\eta_{12} = -9.7 \pm 4.6$. Experiments on the electro–rheological behavior of nematics are analyzed by essentially the same procedure [30].

3.3. Polymeric Liquids

To model a polymer melt, one starts from a simple fluid of spherical particles and introduces extra binding forces or constraints [31, 32], in order to form molecular chains with a prescribed chain length of N_{ch} beads. Fixed bond angles have to be imposed when chains composed of specific chemical units, e.g., of CH_2, are treated. Longer chains can be modelled by freely jointed beads where each "monomer" is a Kuhn element which stands for a few (≈ 3 to 10) chemical units. Here model polymeric liquids of the latter type are discussed.

Rheological studies for LJ-fluids where the binding was achieved by increasing the energy parameter Φ_0 for neighbors in a chain by a factor showed many features of the nonlinear flow behavior typical for polymeric melts [33, 34]. Also thermal degradation and shear induced breaking of chains were observed. The results to be presented here [36] follow from an extension of the previous simulations [35] for a system where all particles interact via the repulsive part of the LJ-potential (WCA) and an attractive FENE potential where the maximum bond length R_0 is used for the

binding within the chains. More specifically, $\Phi = \Phi^{\mathrm{WCA}} + \Phi^{\mathrm{FENE}}$ with $\Phi^{\mathrm{WCA}} := 4\Phi_0[(\frac{r_0}{r})^{12} - (\frac{r_0}{r})^6 + \frac{1}{4}]$, $r \leqslant 2^{1/6} r_0$, and $\Phi^{\mathrm{WCA}} = 0$ for $r > 2^{1/6} r_0$; $\Phi^{\mathrm{FENE}} := -0.5\, k^* \Phi_0 \frac{R_0^2}{r_0^2} \ln[1 - \frac{r^2}{R_0^2}]$, $r \leqslant R_0$, and $\Phi^{\mathrm{FENE}} = \infty$ for $r > R_0$. For this potential with $R_0 = 1.5$, $k^* = 30$, $T = \Phi_0/k_B$, and $nr_0^3 = 0.85$ extensive equilibrium MD-studies have been carried out by Kremer and Grest [37]. In Refs. 35 and 36 and for the data to be considered, the same potential parameters and the same state point are used except for a slightly smaller density of $nr_0^3 = 0.84$. Molecules with chain lengths $N_{ch} = 10$, 30, 60, 100, 150, 200, 300, and 400 were studied.

The Newtonian limit η_{New} of the viscosity, for long molecules was only reached at extremely small shear rates. When studied as a function of the chain length N_{ch}, two regimes, referred to as the Rouse regime, where $\eta_{\mathrm{New}} \sim N_{\mathrm{ch}}$, and as the reptation regime, where $\eta_{\mathrm{New}} \sim N_{\mathrm{ch}}^{3.5}$ can be distinguished. The transition between these regimes occurs at $N_{\mathrm{ch}} \approx 100$. This value is, as expected, about three times the entanglement length of ≈ 35 inferred from equilibrium studies [37]. A procedure to analyze and measure entanglements in MD-simulations is available [38].

Other rheological properties, such as the first and second normal stress differences and the viscometric functions have been computed [35, 36]. The shear induced bond orientation, as it can be measured via the birefringence, as well as the static structure factor of the whole melt or of selectively marked chains and the shape of single polymer chains were analyzed and found to be in good agreement with experiments [39]. Other geometries, such as extensional flow of polymer melts [41] have also been simulated.

Dilute polymer solutions have also been studied under nonequilibrium conditions [32, 42]. In particular, the angle χ specifying the flow orientation of the radius of gyration tensor is studied as function of the shear rate γ. The "shear resistance" m, defined by [43] $\tan(2\chi) = m/\beta$, $\beta = \gamma\tau$, where τ is a relaxation time, is compared with experimental findings. The dependence of m on the shear rate which came as a surprise some time ago, is similar for the real and for the model polymer solutions. For theoretical explanations see Ref. 44. The rotational dynamics of a polymer chain in a shear flow, i.e., tumbling, stretching and folding, can be followed in the NEMD simulation by direct inspection and by computing appropriate time correlation functions.

ACKNOWLEDGMENTS

Financial support by the Deutsche Forschungsgemeinschaft (DFG) via the Sonderforschungsbereiche (SFB 448) "Mesoskopisch strukturierte

Verbundsysteme," (SFB 605) "Elemantarreibereignisse," and the Graduiertenkolleg "Polymerwerkstoffe," the substantial help of C. Aust., L. Bennett, and M. Kröger, as well as the generous donation of computer time by the Konrad-Zuse-Zentrum für Informationstechnik (Berlin) and by the Höchstleistungsrechenzentrum der Kfa Jülich GmbH are gratefully acknowledged.

REFERENCES

1. H. M. Laun, R. Bung, S. Hess, W. Loose, O. Hess, K. Hahn, E. Hädicke, R. Hingmann, F. Schmidt, and P. Lindner, *J. Rheol.* **36**:743 (1992).
2. N. A. Clark and B. J. Ackerson, *Phys. Rev. Lett.* **44**:1005 (1980). B. J. Ackerson, *Physica A* **174**:15 (1991).
3. P. Lindner, *Physica A* **174**:74 (1991).
4. W. T. Ashurst and W. G. Hoover, *Am. Phys. Soc.* **17**:1196 (1972); *Phys. Rev. Lett.* **31**:206 (1972). A. W. Lees and S. F. Edwards, *J. Phys. C* **5**:1921 (1972). G. Ciccotti, G. Jacucci, and I. R. McDonald, *Phys. Rev. A* **13**:426 (1975).
5. W. G. Hoover, *Molecular Dynamics* (Springer, Berlin, 1986). M. P. Allen and D. J. Tildesley, *Computer Simulation of Liquids* (Clarendon, Oxford, 1987). D. J. Evans and G. P. Morriss, *Statistical Mechanics of Nonequilibrium Liquids* (Academic Press, London 1990). R. Haberlandt, S. Fritzsche, G. Peinel, and K. Heinzinger, *Molekular-Dynamik* (Vieweg, Braunschweig, 1995).
6. W. Loose and S. Hess, *Phys. Rev. Lett.* **58**:2443 (1988); *Phys. Rev. A* **37**:2099 (1988).
7. S. Hess and W. Loose, *Physica A* **162**:138 (1989).
8. S. Hess, in *Rheological Modelling: Thermodynamical and Statistical Approaches*, J. Casas-Vázques and D. Jou, eds., Lecture Notes in Physics, Vol. 381 (Springer, Berlin, 1991), p. 51.
9. S. Hess, M. Kröger, W. Loose, C. Pereira Borgmeyer, R. Schramek, H. Voigt, and T. Weider, in *Monte Carlo and Molecular Dynamics of Condensed Matter Systems*, IPS Conf. Proc. 49, K. Binder and G. Ciccotti, eds. (Bologna, 1996), pp. 825–841.
10. S. Hess, in *Computational Physics*, K. H. Hoffmann and M. Schreiber, eds. (Springer, Berlin, 1996), pp. 268–293; in *A Perspective Look at Nonlinear Media—From Physics to Biology and Social Sciences*, Lecture Notes in Physics, Vol. 503, J. Parisi, S. C. Müller, and W. Zimmermann, eds. (Springer, Berlin, 1998), pp. 75–95.
11. D. J. Evans and G. P. Morriss, *Phys. Rev. Lett.* **51**:1776 (1983); *J. Chem. Phys.* **77**:63 (1983); *Phys. Rev. Lett.* **56**:2172 (1986).
12. W. Loose and S. Hess, *Rheol. Acta* **28**:91 (1989). W. Loose and S. Hess, in *Microscopic Simulation of Complex Flows*, M. Mareschal, ed., ASI series (Plenum Press, 1990). S. Hess and W. Loose, *Ber. Bunsenges., Phys. Chem.* **94**:216 (1990).
13. O. Hess, W. Loose, T. Weider, and S. Hess, *Physica B* **156/157**:505 (1989). T. Weider, U. Stottut, W. Loose, and S. Hess, *Physica A* **174**:1 (1991). S. Hess, D. Baalss, O. Hess, W. Loose, J. F. Schwarzl, U. Stottut, and T. Weider, in *Continuum Models and Discrete Systems*, G. A. Maugin, ed. (Longman, Essex, 1990), Vol. 1, pp. 18–30.
14. S. Hess, *Physica A* **118**:79 (1983).
15. S. Hess and H. J. M. Hanley, *Phys. Lett. A* **98**:35 (1983). H. J. M. Hanley, J.C. Rainwater, and S. Hess, *Phys. Rev. A* **36**:1795 (1987). J. C. Rainwater, H. J. M. Hanley, and S. Hess, *Phys. Lett. A* **36**:450 (1988).
16. J. F. Schwarzl and S. Hess, *Phys. Rev. A* **33**:4277 (1986).
17. J. J. Erpenbeck, *Phys. Rev. Lett.* **52**:1333 (1984).

18. S. Hess in D. Quemada, ed., *Nonlinear Behavior of Dispersive Media*, *J. Mécanique Théor. Appl.*, Numéro spécial 1985, pp. 1–19; *Int. J. Thermophys.* **6**:657 (1985); *J. de Physique* **46**, Colloque 3 (C3), Supplement 3: 191 (1985).
19. J. C. Maxwell, *Proc. Roy. Soc. London (A)* **22**:46 (1873); *Pogg. Ann. Physik* **151**:151 (1874).
20. P. G. de Gennes, *The Physics of Liquid Crystals* (Clarendon Press, Oxford, 1974), Chap. 3. H. Kelker and R. Hatz, *Handbook of Liquid Crystals* (Verlag Chemie, Weinheim, 1980). G. Vertogen and W. deJeu, *Thermotropic Liquid Crystals, Fundamentals*, Chemical Physics, Vol. 45 (Springer, Berlin, 1988).
21. J. L. Ericksen, *Arch. Ratl. Mech. Anal.* **4**:231 (1960); *Mol. Cryst. Liq. Cryst.* **7**:153 (1969). F. M. Leslie, *J. Mech. Appl.Math.* **19**:357 (1966); *Arch. Ratl. Mech. Anal.* **28**:265 (1968). O. Parodi, *J. Phys.* **31**:58 (1970).
22. J. B. Gay and B. J. Berne, *J. Chem. Phys.* **74**:3316 (1981).
23. D. J. Adams, G. R. Luckhurst, and R. W. Phippen, *Mol. Phys.* **61**:1575 (1987). E. de Miguel, L. F. Rull, M. K. Chalam, and K. E. Gubbins, *Mol. Phys.* **71**:1223 (1991); **72**:593 (1991); **74**:405 (1991). E. de Miguel, E. Martin del Rio, J. T. Brown, and M. P. Allen, *J. Chem. Phys.* **105**:4234 (1996). E. de Miguel and E. Martin del Rio, *Phys. Rev. E* **55** (1997) 2916.
24. T. Gruhn and M. Schoen, *Phys. Rev. E* **55**:2861 (1997); *Mol. Phys.* **93**:681 (1998); *J. Chem. Phys.* **108**:9124 (1998).
25. S. Sarman and D. J. Evans, *J. Chem. Phys.* **99**:9021 (1993).
26. S. Sarman, *Physica A* **240**:160 (1997); *J. Chem. Phys.* **103**:393 (1995); **107**:3144 (1997).
27. A. M. Smondyrev, G. B. Loriot, and R. A. Pelcovits, *Phys. Rev. Lett.* **75**:2340 (1995).
28. L. Bennett, S. Hess, C. Pereira Borgmeyer, and T. Weider, *Int. J. Thermophys.* **19**:1143 (1998).
29. L. Bennett and S. Hess, *Phys. Rev. E* **60**:5561 (1999).
30. A. Eich, B. A. Wolf, L. Bennett, and S. Hess, *J. Chem. Phys.* **113**:3829 (2000).
31. J. P. Ryckaert and A. Bellemans, *Faraday Disc. Chem. Soc.* **66**:95 (1978). A. Berker, S. Chynoweth, and Y. Michopoulos, NEMD Simulations and the Rheology of Liquid Hydrocarbons, in *Microscopic Simulations of Complex Hydrodynamic Phenomena*, M. Mareschal and B. L. Holian, eds. (Plenum, New York, 1992) pp. 75–88.
32. C. Pierleoni and J. P. Ryckaert, *Phys. Rev. Lett.* **71**:1724 (1993); *Macromolecules* **28** (1995) 5087. J. P. Ryckaert, in *Monte Carlo and Molecular Dynamics of Condensed Matter Systems*, K. Binder and G. Ciccotti, eds. (IPS Conf. Proc. 49, Bologna, 1996), pp. 725–746.
33. S. Hess, *J. Non-Newtonian Fluid Mech.* **23**:187 (1987).
34. M. Kröger and S. Hess, *Physica A* **195**:336 (1993).
35. M. Kröger, W. Loose, and S. Hess, *J. Rheol.* **37** (1993).
36. M. Kröger, *Rheology* **95**:66 (1995).
37. K. Kremer and G. S. Grest, *J. Chem. Phys.* **92**:5057 (1990).
38. M. Kröger and H. Voigt, *Macromol. Theory Simul.* **3**:639 (1994).
39. R. Muller, J. J. Pesce, and C. Picot, *Macromol.* **26**:4356 (1993).
40. S. Hess, C. Aust, L. Bennett, M. Kröger, C. Pereira Borgmeyer, and T. Weider, *Physica A* **240**:126 (1997).
41. M. Kröger, C. Luap, and R. Muller, *Macromol.* **30**:526 (1997).
42. C. Aust, M. Kröger, and S. Hess, *Macromol.* **32**:5660 (1999).
43. A. Link, M. Zisenis, B. Prötzel, and J. Springer, *Makromol. Chem., Macromol. Symp.* **61**:358 (1992).
44. C. Schneggenburger, M. Kröger, and S. Hess, *J. Non-Newt. Fluid Mech.* **62**:235 (1996).